Two-Photon Excitation of Substituted Enediynes

John F. Kauffman*,† and Joseph M. Turner

Department of Chemistry, University of Missouri-Columbia, Columbia, Missouri 65211

Igor V. Alabugin,* Boris Breiner, and Serguei V. Kovalenko

Department of Chemistry and Biochemistry, Florida State University, Tallahassee, Florida 32303

Ekaterina A. Badaeva

Department of Natural Sciences, New Mexico Highlands University, Las Vegas, New Mexico 87701

Artëm Masunov

Nanoscience Technology Center, Department of Chemistry and Department of Physics, University of Central Florida, Orlando, Florida 32826

Sergei Tretiak*

Theoretical Division and Center for Nonlinear Studies Division, Los Alamos National Laboratory, Los Alamos, New Mexico 87545

Received: October 25, 2005

Electronic spectroscopy of nine benzannelated enediynes and a related fulvene was studied under one-photon and two-photon excitation conditions. We utilize measured absorbance and emission spectra and time-resolved fluorescence decays of these molecules to calculate their radiative lifetimes and fluorescence quantum yields. The fluorescence quantum yields for the other compounds were referenced to the fluorescence quantum yield of compound **3** and used to determine relative two-photon absorption cross-sections. Further insight into experimental studies has been achieved using time-dependent density functional (TD-DFT) computations. The probability of two-photon absorption (TPA) increases noticeably for excitation to the higher excited states. The photophysical properties of benzannelated enediynes are sensitive to substitutions at both the core and the periphery of the enediyne chromophore. Considerably enhanced two-photon absorption is observed in an enediyne with donor substitution in the middle and acceptor substitution at the termini. Excited states with B symmetry are not active in TPA spectra. From a practical point of view, this study extends the range of wavelengths applicable for activation of the enediyne moiety from 350 to 600 nm and provides a rational basis for future studies in this field. Our theoretical computations confirmed that lowest energy TPA in benzannelated enediynes involves different orbitals than lowest energy one-photon absorbance and provided further support to the notion that introduction of donor and acceptor substituents at different ends of a molecule increases TPA.

Introduction

The Bergman cyclization[1] of an enediyne moiety to a reactive *p*-didehydrobenzene diradical (**I** → **II**) is the key step in the chemical mechanism responsible for the biological activity of naturally occurring enediyne antibiotics[2] (Scheme 1). The simultaneous formation of *two* radical centers in the *p*-benzyne intermediate is important because it results in abstraction of *two* hydrogen atoms (one from *each* strand of a doubly stranded DNA) which, after a sequence of reactions, ultimately leads to double-stranded DNA cleavage.[3] Unfortunately, despite their highly elaborate architecture, the natural enediynes do not differentiate between healthy and cancer cells and, thus, are extremely toxic. Numerous attempts to achieve higher spatial and temporal control over reactivity have produced much research into the synthesis of analogues of the naturally occurring enediynes.[4,5] This includes attempts to tune the reactivity of the designed enediynes through either strain[6−9] or electronic[10,11] effects and, most recently, to conjugate natural enediynes with monoclonal antibodies.[12] The challenge is that the enediyne has to be relatively stable at ambient temperature to allow resilient handling and drug delivery but needs to become activated at body temperature upon docking to DNA. Unless a special triggering event is used to convert a prodrug to its active form, there is only a small temperature window where reactivity and stability are balanced for thermally activated enediynes.

Photochemical activation is appealing because it provides both spatial and temporal control over drug activation with the drug being harmless until activated by light. Light can be selectively delivered to the right place and at the right time when the concentration of the drug in the tumor is highest without causing damage to the other organs. This explains why considerable efforts have been devoted recently to developing a photochemical version of the Bergman cyclization.[13−20] However, even despite several promising results, little double-stranded (ds) DNA cleavage has been observed for most photochemically triggered Bergman cyclizations of designed enediynes.[21] The efficiency of the photochemical Bergman cyclization is often low, and high-energy tissue-damaging UV radiation is often

* To whom correspondence should be addressed. E-mail: alabugin@chem.fsu.edu; E-mail: kauffmanj@cder.fda.gov; E-mail: serg@lanl.gov.

† Current Address: Food and Drug Administrations, Center for Drug Evaluation and Research, Office of Pharmaceutical Sciences, Division of Pharmaceutical Analysis, 1114 Market St., St. Louis, MO 63101.

10.1021/jp056127y CCC: $33.50 © 2006 American Chemical Society
Published on Web 12/08/2005

SCHEME 1: Two Possible Cyclization Pathways of Enediynes. Hydrogen-atoms (H-atoms) Abstracted from the Environment Are Shown in Italics

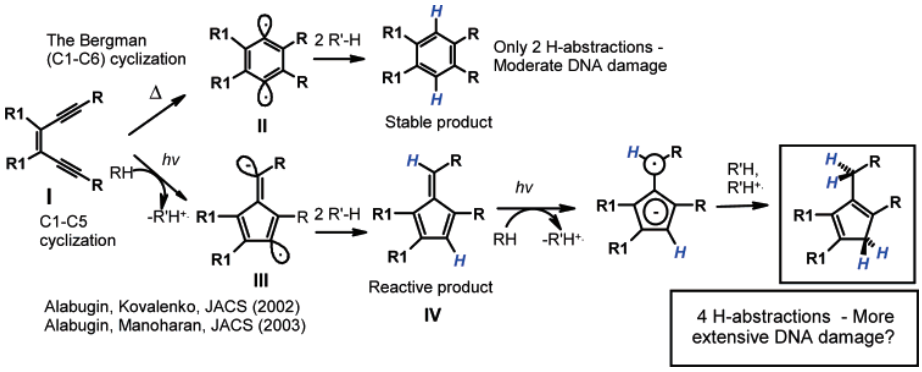

required to initiate it by one-photon absorption (OPA). Dynemicine A, a hybrid antitumor antibiotic activated through bioreduction followed by the normal Bergman cyclization, is the only enediyne which shows considerable DNA cleavage when activated by visible (580 nm) light.[22]

Recently, we have discovered that, with proper modification, the enediyne moiety can undergo a new photoinduced reaction which is different from the Bergman cyclization.[23,24] Upon UV irradiation (300−350 nm) in the presence of 1,4-cyclohexadiene in acetonitrile, the bis-tetrafluoropyridinyl (TFP) enediynes undergo photochemical transformation into a mixture of isomeric indenes. We have prepared the proposed fulvene intermediate through Bu_3Sn radical-mediated 5-exo-cyclization of enediynes[25] and found that, unlike the benzene product of the Bergman cycloaromatization cascade which is stable, the fulvene is indeed capable of further photoreduction to indene.[26] As a result, the new photochemical pathway ultimately leads to *four* formal hydrogen atom abstractions, with the potential to effectively double the DNA-damaging ability of the Bergman cycloaromatization pathway (Scheme 1). The new pathway is available only when enediynes are photochemically activated in the vicinity of a suitable electron donor such as DNA. Without such a donor, the newly developed enediynes are thermally and *photochemically* inert. We prepared water-soluble enediynes equipped with DNA-recognition elements and found them to be efficient ds DNA photocleavers. Statistical analysis of DNA cleavage unambiguously shows that lysine−enediyne conjugates induce 100 times more ds DNA cleavage than expected from a combination of random coincident single-stranded (ss) cleavages[27] and that they have ds/ss DNA cleavage ratios comparable to those of bleomycin.[28]

A necessary condition for utilizing photochemistry of enediynes for practical purposes is a thorough understanding of photophysical processes involving an enediyne moiety. In particular, their two-photon absorbance[29] (TPA) activities are especially important because TPA allows one to reach a high-energy excited state via *simultaneous* absorption of two photons of lower energy. Two-photon activation is especially promising in cancer phototherapy[30,31] when low-energy photons can be delivered through the therapeutic optical window of tissues. As an additional benefit, the quadratic dependence of the two-photon absorption cross-section on light intensity ensures excellent three-dimensional spatial control over the location of the treated tissue and minimal photodamage to healthy tissue.

In this article, we explore the basic photophysical factors needed to lay the foundation for using the TPA technique to initiate the enediyne cyclization reactions. Practical therapies based on two-photon excitations would require the enediynes to have significant TPA cross-sections.[32] We examine the photophysical properties of a series of nine substituted enediynes and a related compound shown in Figure 1. We utilize measured absorbance and emission spectra and time-resolved fluorescence decays of these compounds to calculate their radiative lifetimes and fluorescence quantum yields. The results demonstrate that the quantum yields are independent of excitation wavelength. We also present two-photon excited fluorescence (TPEF) spectra for several of these compounds. The integrated TPEF spectra along with the fluorescence quantum yields are used to estimate

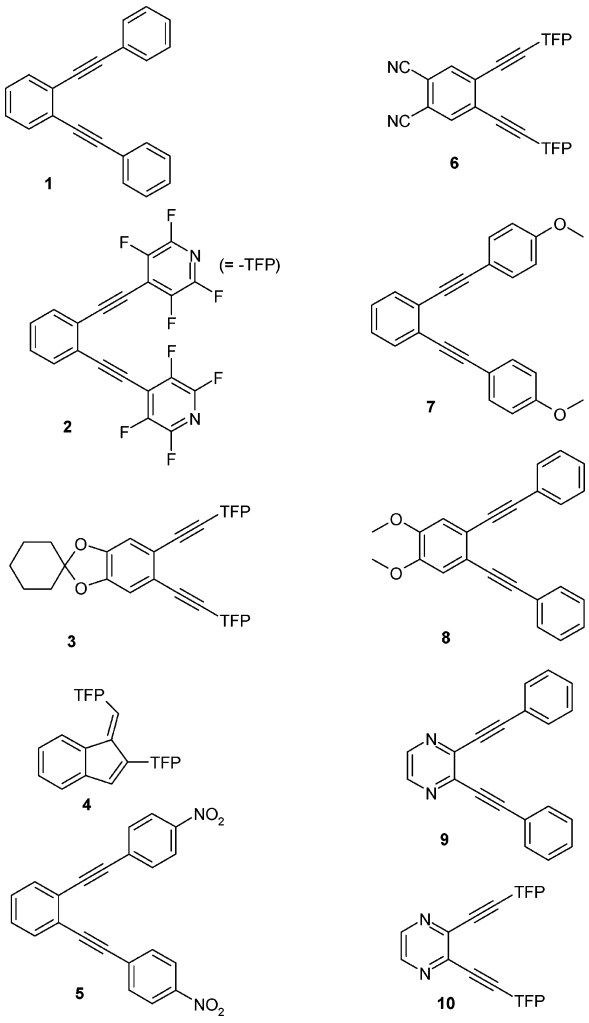

Figure 1. Structures of compounds **1** − **10**.

relative two-photon absorption cross-sections for the enediynes. The results were analyzed using TD-DFT computations that provided a further insight into the nature of the excited state involved in the OPA and TPA processes and confirmed all observed experimental trends.

Experimental Section

Preparation of Compounds 1−10. Compounds **1**, **2, 4**, **5**, **7**, **8**, and **10** were prepared according to literature procedures.[23,25,33] Compounds **3**, **6**, and **9** were synthesized analogously.[34] Enediyne **9** was prepared by Sonogashira coupling of 2,3-dichloropyrazine with phenylacetylene. The tetrafluoropyridinyl- (TFP-) substituted enediynes were obtained by Sonogashira coupling of tetramethylsilylacetylene with the respective diiodobenzenes or 2,3-dichloropyrazine, followed by in situ deprotection/substitution of the resulting TMS-protected enediynes with CsF and pentafluoropyridine.[35] Fulvene **4** was synthesized from enediyne **2** by tin-radical-initiated cyclization, followed by hydrolysis with HCl.[25]

Absorbance and emission spectra were recorded in quartz cuvettes containing a 6.0×10^{-6} M solution of the compound under study in acetonitrile. Acetonitrile (Fisher, HPLC grade) was used as received. Absorbance spectra were collected on a HP 8453 diode array spectrometer with 1 nm resolution. Emission spectra were collected on a Varian Eclipse fluorometer in excitation−emission−matrix (EEM) mode. Emission spectra were collected from 250 to 650 nm at 2 nm intervals, with a 2.5 nm band-pass. These spectra were taken using excitation wavelengths from 230 to 400 nm at 10 nm intervals and a 2.5 nm excitation band-pass. Each compound exhibited a series of excitation wavelength-independent emission spectra which intensities were scaled with the absorbance at the excitation wavelength. Time-resolved emission decays were measured by the time-correlated single photon counting method with 300 nm excitation. The excitation source was a 4 MHz frequency-doubled, synchronously pumped, cavity-dumped dye laser having a pulse width of ∼2 ps. The dye laser was pumped by the frequency-doubled output of an 80 MHz mode-locked, diode-pumped Nd:YAG laser of our own design. The instrument was calibrated to 0.010 ns per channel using a coaxial cable of known time delay, and the instrument response function was 80 ps (fwhm), which was determined by measuring the signal from a scattering solution through a 300 nm band-pass filter. The temperature was maintained at 25.0 °C using a Peltier thermoelectric cuvette holder. Multiexponential model fluorescence decay functions were extracted from measured fluourescence decays using iterative reconvolution software of our own design based on the Marquardt−Levenberg algorithm for the minimization of χ^2. The analysis presented below is based on fluorescence decays measured from 6.0×10^{-6} M solutions of the enediynes. Fluorescence decays from 2.0×10^{-3} M were also measured using a triangular, quartz front surface cell and found to be identical to the decays from the micromolar solutions. Therefore, it is permissible to use quantum yields derived from the micromolar solution decays to determine the relative TPA cross-sections from integrated two-photon excited fluorescence spectra.

TPEF spectra of 2×10^{-3} M solutions of compounds **1−10** in acetonitrile were measured on a spectrometer of our own design. The femtosecond laser source for the spectrometer is a Clark-MXR CPA-2000 chirped pulse amplified Ti:Sapphire laser. The system produces 775 nm light at a 1000 Hz repetition rate. The typical pulse width is 120−150 fs (full width at half maximum, fwhm) as measured by interferometric autocorrelation. The 775 nm light is directed into an optical parametric amplifier (Clark-MXR vis-OPA), to generate femtosecond laser pulses tunable from 450−700 nm and an average power of approximately 3 mW at the sample. (Internal OPA optics include a frequency-doubling crystal to generate the 388 nm OPA pump beam and a white-light generator to seed the OPA.) The spectral bandwidth of the output of the OPA is approximately ±2.5 nm. TPEF spectra were collected with a computer-controlled motorized monochromator (ISA H-10, reciprocal linear dispersion = 8 nm/mm, 0.5 mm slits) and a Hamamatsu R928 PMT situated perpendicular to the excitation beam. The PMT signal was sampled and held and delivered to an analog-to-digital converter (Data Translation DT2812) and was integrated over 1000 excitation pulses and recorded for each emission wavelength at 2 nm intervals to obtain a multiphoton excited fluorescence spectrum. The excitation wavelength was varied for each compound as described in the text below. Excitation intensity was monitored with a calibrated photodiode and controlled with a motorized circular variable density filter. Excitation wavelength was monitored with a fiber-coupled diode array spectrometer (Ocean Optics).

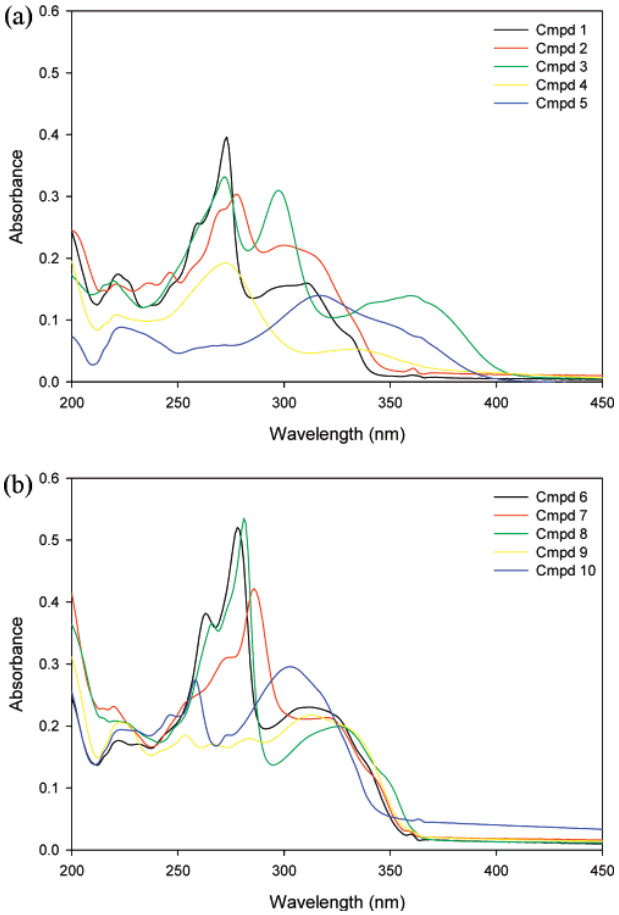

Figure 2. (a) Experimental OPA spectra of compounds **1−5**. (b) Experimental OPA spectra of compounds **6−10**.

Electronic Spectroscopy of Enediynes and Related Compounds. Figure 2 presents the absorbance spectra of compounds **1−10**. All molecules have two major distinguishable absorption peaks labeled S1 and S2, respectively. With the exception of compounds **4** and **5**, all spectra exhibit discernible S1 states with peaks in the 300 to 360 nm range. Estimates of the S1 peak absorbance wavelengths are reported in Table 1.

TABLE 1: Features in the Absorbance and Emission Spectra of Enediynes and Related Compounds

	absorbance					emission		
compound	S1 λ_{peak}	λ_{max} (nm)	A (λ_{max})	A (270 nm)	A (300 nm)	λ_{max} (nm)	F (λ_{max})	fwhm (nm)
1	310	273	0.396	0.351	0.155	360	75	65
2	300	278	0.303	0.278	0.221	370	125	60
3	360	272	0.332	0.323	0.299	460	160	75
4	335	272	0.193	0.190	0.062	395	0.15	~60
5	350	320	0.140	0.059	0.106			
6	315	278	0.520	0.374	0.213	370	80	60
7	320	286	0.422	0.301	0.222	380	150	65
8	325	281	0.535	0.357	0.147	380	105	60
9	315	313	0.217	0.167	0.192	380	14	60
10	305	303	0.296	0.172	0.293	440	0.55	~100

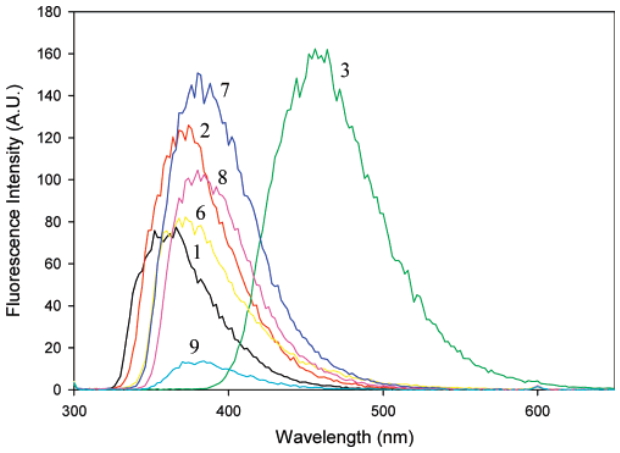

Figure 3. Measured fluorescence spectra of compounds **1**−**3**, and **6**−**9**.

Compound **4** exhibits a discernible peak in this region, but it is not well distinguished from transitions to the higher excited states. Distinct S1 and S2 features are not observed in the spectrum of compound **5**, and as a result, the S1 absorbance peak is not resolved. With the exception of compound **5**, all of the spectra show strong absorbances to the blue of their putative S1 peak wavelengths. Absorbances to higher excited states are larger than the S1 absorbances for all of the compounds except compounds **5**, **9**, and **10**. Table 1 gives the maximum absorbance and wavelength of maximum absorbance for each compound. The absorbances at 300 and 270 nm have also been tabulated. These values will be useful for subsequent discussions.

Fluorescence spectra of compounds **1**−**3** and **6**−**9** are shown in Figure 3, and the emission features of all 10 compounds are summarized in Table 1. The excitation wavelength for these spectra is 300 nm. Compounds **4** and **10** exhibit extremely weak fluorescence that is not intense enough to be observed on the ordinate scale in Figure 3. Compound **5** produces no measurable fluorescence. The remaining seven compounds exhibit similar fluorescence spectra, with distorted Gaussian peaks and bandwidths (fwhm) of about 60 nm. Their peaks are in the range of 360 to 385 nm. Compounds **3** and **10** are exceptions, with peaks at 460 and 440 nm and bandwidths of 75 and ~100 nm, respectively. These two compounds also exhibit larger Stokes shifts (~100 nm) compared to the ~60 nm shifts observed for the other seven compounds. This may be attributed to solvatochromic effects: apparently, the combination of TFP substituents and ring heteroatoms confers a stronger solvent sensitivity to these two compounds. None of these spectra shows strong vibronic structure. Shoulders are evident on the rising edges of some of the absorbance spectra, most noticeably the spectrum of compound **1**. The emission spectra of these compounds also exhibit subtle shoulders, particularly compound **1**. This observation suggests that a mirror symmetry relationship may exist between the absorbance and emission spectra, and the assumption of a mirror symmetry relationship may be a useful metric for estimating the shape of the S1 band absorbance spectra of these compounds.

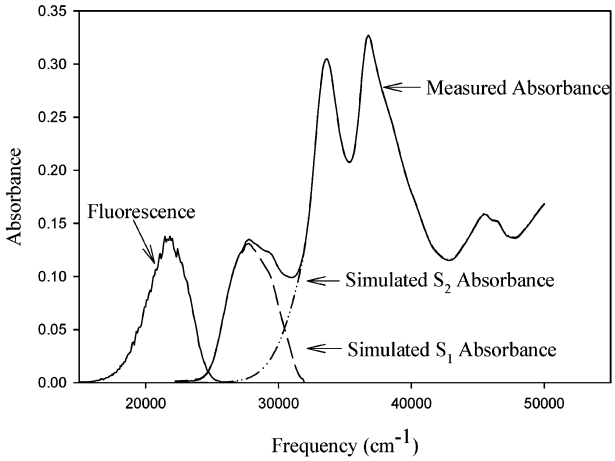

Figure 4. Simulated spectrum of compound **3**.

TABLE 2: Fluorescence Decay Parameters for Enediynes in Acetonitrile

	fluorescence decay parameters					
compound	amplitude	time const. (ns)	χ^2 (relative)	τ_{rad} (ns)	quantum yield	st. dev. (vs λ)
1	0.919	1.467	1.482	2.8 ± 0.4	0.52 ± 0.08	0.04
2	0.940	1.812	0.832	2.9 ± 0.4	0.63 ± 0.09	0.03
3[a]	0.940	5.300	1.040	5.9 ± 0.6	0.9 ± 0.1	0.06
4	0.120	2.218	0.429		0.01 ± 0.003	0.004
	0.821	0.041				
5	NO	EMISSION				
6	0.937	3.920	1.150	8.0 ± 1	0.49 ± 0.07	0.03
7	0.948	2.143	0.951	2.6 ± 0.4	0.83 ± 0.12	0.06
8	0.957	2.095	0.935	2.6 ± 0.4	0.81 ± 0.12	0.08
9	0.528	0.456	0.489		0.07 ± 0.02	0.006
	0.483	0.198				
10	0.043	5.530	0.654		0.011 ± 0.003	
	0.846	0.472				

[a] The radiative lifetime of compound **3** is calculated using the Strickler−Berg model, and its quantum yield is calculated from the Strickler−Berg lifetime and the measured fluorescence lifetime. All other quantum yields are determined from the integrated fluorescence spectra using compound **3** as reference. All other radiative lifetimes are calculated from quantum yields and measured lifetimes.

We have chosen to use compound **3** as a reference for quantum yield determinations, because it appears to have the best resolved S1 state and because its emission band appears to be more Gaussian in shape than the other compounds, owing to its more slowly varying rising edge (Figure 4). We have measured the quantum yield of compound **3** from its integrated fluorescence spectrum and the absorbance at the excitation wavelength using perylene in hexane ($\phi_{fl} = 0.94$) as a reference. Compound **3** has a quantum yield of 0.86 determined by this method.

Fluorescence Lifetimes of Enediynes and Related Compounds. Time-resolved fluorescence decays for each of the compounds were measured following 300 nm excitation, and the best fitting parameters for the multiexponential model functions are tabulated for each compound in Table 2. The emission wavelength was 370 nm for all decays except compound **3**, which was measured at 420 nm, and compound **10**, which was measured at 460 nm. The uncertainty in the time constants is estimated as ±5%, based on the sensitivity analysis performed during the fitting procedure. The table also gives

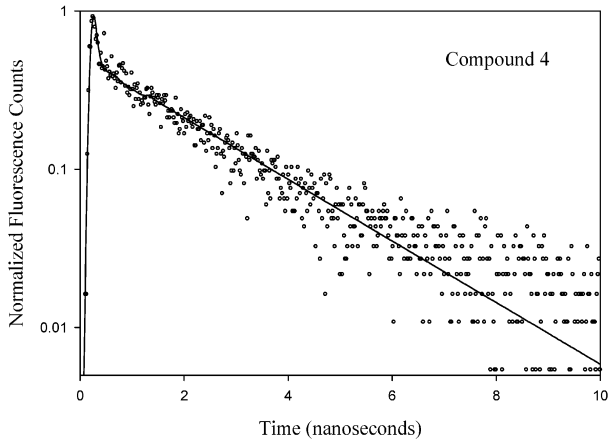

Figure 5. Fluorescence decay of compound **4** at 370 nm. The best-fit model function convoluted with the instrument function is also shown. The ordinate scale is logarithmic, and the decay is biexponential. The instrument function has been omitted for clarity. See Figures 6 and 7 for typical instrument functions.

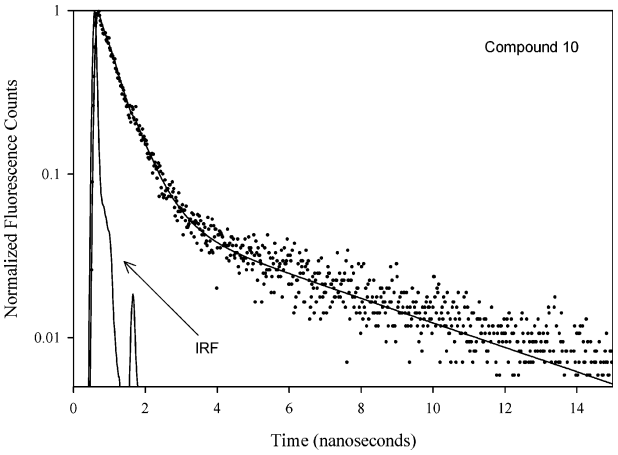

Figure 6. Fluorescence decay of compound **10** at 370 nm. The instrument response function (IRF) and the best-fit model function convoluted with the instrument function are also shown. The ordinate scale is logarithmic, and the decay is biexponential.

values of χ^2 (relative) for each fit. The relative χ^2 values are close to unity (1 ± 0.3), with the exception of the fit for compound **1**. There is some evidence for a fast decay component that might represent a small (amplitude 0.03) scattered light contamination or a fast relaxation process, but the time constant for the major decay component does not change when a second exponential is added to the model function. The nitro enediyne **5** showed no emission, and its fluorescence decay was pure noise. Scattered light was not apparent in its emission decay scan. The decay of fulvene **4**, though weak, exhibits unambiguous biexponential character, as shown in Figure 5. The magnitude of the fast decay component is too large to be scattered by 300 nm photons from the excitation source, and this data suggests that fulvene undergoes a fast nonradiative decay to a nonradiative state that is in equilibrium with the emissive S1 state. The bis-TFP pyrazine derivative **10** also exhibits unambiguous biexponential character, and its fluorescence decay is shown in Figure 6. The data suggests that compound **10** also relaxes to a nonradiative state that is in equilibrium with the S1 state. Finally, the fluorescence decay of bis-Ph pyrazine **9** is biexponential too, with time constants that only differ by a factor of 2. Both decay constants are subnanosecond, and the fluorescence decay appears to be single

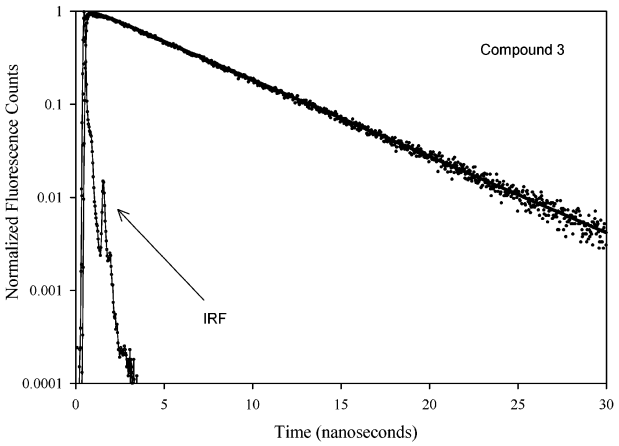

Figure 7. Fluorescence decay of compound **3** at 420 nm. The instrument response function (IRF) and fitted model function are also shown. The ordinate scale is logarithmic, and the decay is single exponential. The fit of the model to data is typical of the measured fluorescence decays.

exponential to the eye. However, fitting with a graphic least-squares fitting program indicates unambiguously that the decay cannot be adequately fit with a single-exponential model function.

The fluorescence decay of compound **3** is shown in Figure 7. It is single exponential in character, and the single-exponential fit is typical of the measured fluorescence decays with the exception of compounds **4**, **9**, and **10**. Its fluorescence lifetime in acetonitrile is 5.3 ns. Solvent-dependent effects upon the fluorescence decays have been observed, and these will be presented in a future paper.

Radiative Lifetime of Enediyne 3. The radiative lifetime of compound **3** in acetonitrile was estimated using the Strickler−Berg formula, which requires a fluorescence spectrum, an absorbance spectrum at known concentration, and solvent refractive index as inputs. The Strickler−Berg model is a generalization of the Einstein A coefficient for spontaneous emission that can be applied to broad molecular absorption and emission bands for strongly absorbing ($\epsilon > 8000$) molecules. The radiative lifetime is related to the absorbance and emission spectra via the expression

$$\frac{1}{\tau_r} = 2.880 \times 10^{-9} n^2 \langle \bar{\nu}_f^{-3} \rangle_{Avg}^{-1} \frac{g_l}{g_u} \int \epsilon(\bar{\nu}) \cdot d \ln(\bar{\nu}) \qquad (1)$$

where n is the refractive index of the solvent, $\bar{\nu}_f$ is the frequency in wavenumbers of the emission signal, the g values are the degeneracies of the upper and lower states for the transition, $\epsilon(\bar{\nu})$ is the molar extinction coefficient of the absorbing species, and $\bar{\nu}$ is the frequency in wavenumbers of the absorbance having extinction coefficient $\epsilon(\bar{\nu})$. The quantity 2.880×10^{-9} is computed from fundamental constants and conversion factors for the radiative lifetime in seconds and frequency in wavenumbers. The fluorescence spectrum is used to calculate $\langle \bar{\nu}^{-3} \rangle_{Avg}^{-1}$, which is a measure of the centroid of the emission peak. The integral over the molar extinction coefficient is calculated using the absorbance spectrum and the concentration. This integral accounts for the majority of the uncertainty in the estimate of the radiative lifetime of compound **3**, because the high-energy band edge of the absorbance spectrum must be estimated in the presence of absorbance to higher excited electronic states, as discussed above. We have estimated the high-energy band edge of the S1 state by the following

procedure, which utilizes the expected mirror symmetry between the S1 absorbance spectrum and the fluorescence spectrum of compound **3**. We assume that the low-energy edge of the S2 state has a Gaussian shape. We append a Gaussian rising edge to the feature whose peak is 33445 cm^{-1} (299 nm) and estimate this as the onset of absorbance to higher excited states of compound **3**. The parameters for the simulated Gaussian rise of S2 are 35000 cm^{-1} peak and 1800 cm^{-1} standard deviation. The amplitude of the Gaussian is adjusted such that it matches the spectrum at 31850 cm^{-1}, and it is grafted onto the absorbance spectrum at this frequency. We then subtract the estimated absorbance to higher excited states from the measured spectrum to give an estimate of the S1 absorption band. The spectral decomposition that results from method 2 is presented in Figure 4. The bandwidth of the resulting spectrum is 4145 cm^{-1}, which is 12% larger than the 3700 cm^{-1} bandwidth of the emission band. This method has the advantage that it retains structure on the high-energy side of the S1 absorbance band, but the band probably terminates more quickly than might be anticipated from the emission spectrum. Using this model, we find that $k_{rad} = 1.69 \times 10^8\ s^{-1}$ for a radiative lifetime of $\tau_{rad} =$ 5.93 ns. The fluorescence quantum yield of compound **3** calculated from the radiative and fluorescence lifetimes is 0.894, which agrees well with the value measured against the perylene reference.

The primary source of uncertainty for the quantum yield calculation is in the estimate of the S1 band shape for compound **3**. We have performed a sensitivity analysis of the quantum yield upon the model used for the high-energy band edge of the absorption spectrum used in the Strickler−Berg calculation. Variations in the Gaussian parameters used to simulate the band edge result in quantum yields that span the range from 0.83 to 0.90. When we use a model that assumes that the high-energy tail of the simulated S1 band is Gaussian, the quantum yield spanned the range from 0.92 to 0.96, depending on the parameters used in the Gaussian assumption. The most reasonable assumptions in both models resulted in quantum yields between 0.87 and 0.92. Sensitivity analysis indicates that the uncertainty in the Strickler−Berg integral is 10%, and therefore, we assign an uncertainty of 10% to the radiative lifetime of compound **3**. Propagation of uncertainty in the quantum yield calculation results in a standard deviation of 0.10. Thus, we report the radiative lifetime and quantum yield for compound **3** as 5.9 (±0.6) ns and 0.9 ± 0.1, respectively. These values are presented in Table 2.

Quantum Yields and Radiative Lifetimes of Enediynes. The requirements of the Strickler−Berg model restrict its applicability in cases where the S1 absorbance band is not well resolved. In lieu of applying this method with all of its caveats to the remaining enediynes and related compounds, we have chosen to use the calculated quantum yield of compound **3** as a reference, against which the quantum yields of the other compounds will be measured. This is appropriate, because the absorbance and emission spectra of these compounds are similar to one another and because the absorbance and emission measurements used in the calculations for all 10 compounds have been measured over a period of ∼3 h. Quantum yields for the remaining compounds have been calculated from the equation

$$\int F^{fl}(\bar{\nu})\cdot d\nu = \Theta^{fl}\cdot K(1 - 10^{-A(\lambda_{ex})}) \qquad (2)$$

where Θ^{fl} is the fluorescence quantum yield, K is an instrument constant that is the product of the excitation power and the collection efficiency function, and A is the absorbance at the excitation wavelength. We determine the instrument constant from eq 2 using the quantum yield of compound **3** and the integrated fluorescence spectrum of compound **3** excited at 360 nm. This wavelength was chosen to be certain that only the S1 state is excited. (Note, however, that we have determined that the quantum yield is wavelength independent, as discussed below.) We estimate the uncertainty of the integrated intensity as 7%, and propagation of uncertainty indicates that K has an uncertainty of 13%.

To test the excitation wavelength dependence of the instrument constant, we used the value of K determined at 360 nm, the excitation wavelength-dependent integrated emission spectra, and the known absorbance of compound **3** at each excitation wavelength. Using these parameters and solving eq 2 for the quantum yield allows us to determine wavelength-dependent quantum yields for compound **3**. We find that the excitation wavelength-dependent variation in the calculated quantum yield is characterized by a mean of 0.89 and a standard deviation of 0.05. The wavelength-dependent variation of the fluorescence quantum yield for compound **3** is less than the 11% uncertainty in the quantum yield derived from the Strickler−Berg model. Thus, the quantum yield for compound **3** is independent of excitation wavelength, within the uncertainty of the measurement.

The wavelength independence of the quantum yield of compound **3** implies that the instrument constant is also wavelength independent, within the uncertainty of the determination. Thus, we are now in a position to utilize the instrument constant to determine the quantum yields of the other nine compounds under investigation. In effect, we are measuring quantum yields relative to that of compound **3** by this procedure. The quantum yields thus determined have been tabulated in Table 2, along with the standard deviation of the variation with respect to wavelength for each compound. Propagated uncertainties in the quantum yield values for compounds **1**, **2**, **6**, **7**, and **8** indicate uncertainties of 15%. As the fluorescence intensity diminishes, the relative contribution of noise to the integrated fluorescence intensity increases. Thus, we estimate that the uncertainty in the quantum yields for compounds **4**, **9**, and **10** may be as high as 30%. In all cases, the variation with wavelength is less than the 11% uncertainty in the value of the quantum yield of compound **3**, and so we conclude that the quantum yields of all of the compounds under study are independent of excitation wavelength within the experimental error. Radiative lifetimes for the compounds under study have also been calculated using the quantum yields and the measured fluorescence lifetimes, and these are tabulated in Table 2. Radiative lifetimes have not been reported for compounds **4**, **9**, and **10**, because they exhibit biexponential decay, which makes the determination of fluorescence lifetime ambiguous.

Two-Photon Excited Fluorescence from Enediynes and Related Compounds. Two-photon excited fluorescence (TPEF) spectra have been measured for all 10 compounds under investigation. When an excitation wavelength of 600 nm was used, only compound **3** exhibited measurable emission. However, when we tuned the femtosecond excitation source to a wavelength equal to twice the wavelength of the peak absorbance of the putative S2 manifold, we observed two-photon excited emission from compounds **1**−**3** and **6**−**9** via two-photon absorbance by the S2 (or higher) state of the molecules under study. Table 3 gives the specific excitation wavelengths used for each compound. Most of the compounds are excited into

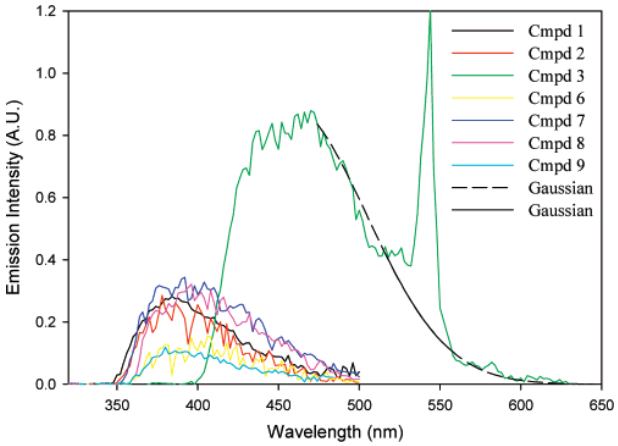

Figure 8. Two-photon excited fluorescence spectra of enediynes.

TABLE 3: Two-Photon Excited Fluorescence of Enediynes and Related Compounds

compound	excitation λ nm	$\lambda_{ex}/2$ nm	relative TPEF intensity	relative quantum yield	$\delta_n^{TPA}/\delta_3^{TPA}$
1	542	271	0.32	0.58	0.55 ± 0.09
2	553	277	0.26	0.7	0.37 ± 0.06
3	542	271	1.00	1.00	1 ± 0.17
4	542	271			
5	458	229			
6	553	277	0.14	0.54	0.26 ± 0.04
7	565	283	0.42	0.92	0.46 ± 0.08
8	565	283	0.35	0.9	0.39 ± 0.07
9	504	252	0.11	0.082	1.34 ± 0.23
10	514	257			

the state near 270 nm, and their one-photon absorbances at this wavelength are tabulated in Table 1.

Thus, it appears that only S2 or higher lying excited states of the molecules in question results in two-photon allowed transitions. The S1 state does not show up in the TPA spectra, even though it makes a notable contribution to the OPA spectra. Quantum-chemical calculations given below will investigate whether the S1 state is forbidden in the TPA activities of these molecules. Examination of the absorbance spectrum of compound **3** indicates that it is the only molecule in this series that has S2 absorbance at 300 nm. Thus, it should come as no surprise since only compound **3** exhibits TPEF with 600 nm excitation.

The TPEF spectra are displayed in Figure 8, and they are essentially identical to the one-photon emission spectra, though some differences are evident due to the fact that the spectra are recorded on different instruments. The relative values of measured integrated fluorescence intensities are tabulated in Table 3. All spectra are truncated after 500 nm to eliminate the excitation line, with the exception of the spectrum of enediyne **3** which extends beyond the 542 nm excitation line. To integrate this spectrum, the excitation spike in the spectrum was smoothed by fitting the entire low-energy band edge to a Gaussian band shape and then grafting it onto the region containing the excitation line. The Gaussian band shape is shown in Figure 7, with the dashed region depicting the overall fit to the band edge and the solid portion depicting the piece that is grafted onto the emission band during integration.

The integrated intensity of the MPEF spectrum of compound n is related to the two-photon absorbance cross-sections for the compound by the expression[36]

$$\int \mathrm{MPEF}_n(\bar{\nu})\cdot d\nu = \Theta_n^{fl}\cdot K^{(2)} g^{(2)} \langle F\rangle^2 \delta_n^{TPA} C_n \qquad (3)$$

where Θ_n^{fl} is the fluorescence quantum yield of compound n, $K^{(2)}$ is the instrument collection constant for the MPEF instrument, $g^{(2)}$ is the second-order temporal coherence factor, $\langle F\rangle^2$ is the square of the spatiotemporally averaged photon flux, δ_n^{TPA} is the TPA cross section of compound n, and C_n is the concentration of compound n. The factor $K^{(2)}g^{(2)}\langle F\rangle^2$ is an instrumental factor that is generally difficult to measure. However, the parameters are expected to be constant for the measured MPEF spectra of the enediynes, because the measurement conditions and spectral ranges of these compounds are very similar. The laser power was adjusted to maintain fixed photon flux for all spectra, and all spectra were measured within a time period of a few hours. The quantum yields are known from the one-photon excited fluorescence measurements, and the concentrations of all samples for MPEF measurements were identical. By the use of compound **3** as a reference, the relative TPA cross-section can be characterized using the expression

$$\frac{I_n^{MPEF}}{I_3^{MPEF}}\frac{\Theta_3^{fl}}{\Theta_n^{fl}} = \frac{\delta_n^{TPA}}{\delta_3^{TPA}} \qquad (4)$$

where $I_n^{MPEF} = \int \mathrm{MPEF}_n(\bar{\nu})\cdot d\nu$, and the subscripts 3 and n refer to the quantities for compound **3** and compound n, respectively. Values for relative integrated intensities (I_n^{MPEF}/I_3^{MPEF}) and relative quantum yields ($\Theta_n^{fl}/\Theta_3^{fl}$) are given in Table 3. The ratio of the integrated TPEF intensity to the quantum yield of each compound provides a relative measure of the TPA cross-section, $\delta_n^{TPA}/\delta_3^{TPA}$, and these are also given in Table 3. Propagated uncertainties indicate that the uncertainty in this quantity is ~17%. According to these measurements, the TPA cross-sections for these compounds increase in the order **6** < **2** < **8** < **7** < **1** < **3** < **9**. The estimate for compound **9** should be accepted with caution, because both its quantum yield and its integrated TPEF intensity are very small and each quantity has substantial uncertainty. Nevertheless, this calculation indicates that, though compound **9** has a very small fluorescence quantum yield, it may have a relatively large TPA cross-section. This calculation indicates that the TPA cross-section for compound **1** is only 55% of that for compound **3**. In view of the large difference between the TPEF intensities of these compounds shown in Figure 8, this result appears to be consistent with experimental observation.

Cross-sections discussed above are relative and determined for a single-excitation wavelength because our current experimental capabilities make measurements of the complete TPA spectra and absolute cross-sections impossible. To complement the experimental studies, test the validity of the observed trends over the broader range of excitation energies, and achieve further insights in the fundamental factors controlling photophysics of enediynes, we resorted to the theoretical analysis of OPA and TPA spectra in these molecules using TD-DFT computational formalism.

Computational Methodology. Quantum-chemical computations have become a powerful tool for insightful theoretical investigations in virtually every molecular class. In particular, adiabatic TD-DFT in the Kohn−Sham (KS) form is currently the method of choice for calculating the excited-state structure of large molecular systems.[37−39] TD-DFT extension for the calculations of molecular nonlinear optical properties based on quasi-particle formalism of the TD-KS equations[40] has shown an excellent quantitative performance of TD-DFT based on hybrid functionals for both OPA and TPA properties.[40,41]

We start our calculations with optimization of ground-state geometries at the Hartree−Fock (HF) level and 6-31G basis

set. This approach usually provides geometries which agree well with experimental X-ray diffraction data[40] in the case of small conjugated substituted molecules. TD-DFT formalism implemented in the Gaussian 98 program package[42] was then used in combination with the hybrid B3LYP exchange-correlation functional and 6-31G basis set to calculate the excited-state electronic structure. Previously, we found that such combination provided fairly accurate results for excited-state structure and optical responses in many molecular structures.[40,41] Frequency-dependent linear and two-photon absorption spectra of compounds **1**−**10** were simulated using the approach described in detail previously.[40] We used the modified collective electronic oscillator (CEO) program[43,44] to calculate first- and third-order polarizabilities $\alpha(\omega, \omega)$ and $\gamma(-\omega, \omega, \omega, -\omega)$ based on the Gaussian 98 output. One-photon absorption intensity at frequency ω is given by the imaginary part of

$$\alpha(\omega) = \sum_{\nu} \frac{2\Omega_{\nu}\mu_{g\nu}}{\Omega_{g\nu}^2 - (\omega + i\Gamma)^2} \tag{5}$$

where $\mu_{g\nu}$ is the dipole moment corresponding to the $|g\rangle$ to $|\nu\rangle$ electronic transition, $\Omega_{g\nu}$ is the vertical transition frequency, and Γ is the line width, assumed to be an empirical value of 0.1 eV for all our calculations. Two-photon absorption cross-section σ_{TPA} is a function of the imaginary part of the third-order frequency-dependent polarizability $\gamma(-\omega, \omega, \omega, -\omega)$[40,43]

$$\sigma_{TPA}(\omega) = \frac{4\pi^2\hbar\omega^2}{n^2c^2} L^4 \mathrm{Im}\langle\gamma\rangle \tag{6}$$

where $\hbar$ is Plank's constant, n is the refractive index of the medium, c is the speed of light, L is the local field factor, calculated in the spherical cavity approximation, and

$$\langle\gamma\rangle = \frac{1}{15}\left(3\sum_{i}\gamma_{iiii} + \sum_{j\neq i}\left(\gamma_{iijj} + \gamma_{ijij} + \gamma_{ijji}\right)\right) \tag{7}$$

is the orientational average of the polarizability tensor γ, where indices i and j refer to the spatial directions x, y, and z. $\gamma(-\omega; \omega, \omega, -\omega)$ has been calculated using the density matrix formalism for nonlinear optical responses recently derived for TD-HF and TD-DFT methodologies as described and implemented in refs 40 and 44.

The first 12 singlet excited states were taken into account in all calculations. In the previous study of similar conjugated molecules, we found 11 states to be sufficient to reach asymptotic values in resonant third-order response properties within 10%.[40] To evaluate solvent effects, we use the polarizable continuum model (PCM) based on the intergral equation formalism (IEF), as implemented in Gaussian 98.[42] Electronic structures have been calculated for selected compounds in the presence of toluene ($\epsilon = 2.4$). Solvent-induced trends (decrease in excitation energies and increase in TPA cross-sections) remained the same when other versions of PCM were used.

Results of OPA and TPA Calculations. The results of theoretical simulations for the OPA spectra are presented in Figure 9. Table 4 provides a comparison of calculated and experimental data. Calculations clearly recover two absorption maxima generally observed in experiment for every compound. The higher energy maximum typically has higher intensity. The excitation energies agree well with the experiment. In all molecules, the ground-state wave function has A symmetry. In most compounds, the low-energy peak corresponds to the first excited state of B symmetry. In compounds **3** and **4**, the second excited state contributes to the first peak as well. For pyrazines **9** and **10** only, the lowest observed OPA state (S1 in our notation) has A symmetry and corresponds to the excitation to the third excited state. Since all the molecules studied have axial rather than central symmetry, both transitions conserving and changing symmetry are dipole allowed in the linear optical response. In the case of A−A excitation, the transition dipole

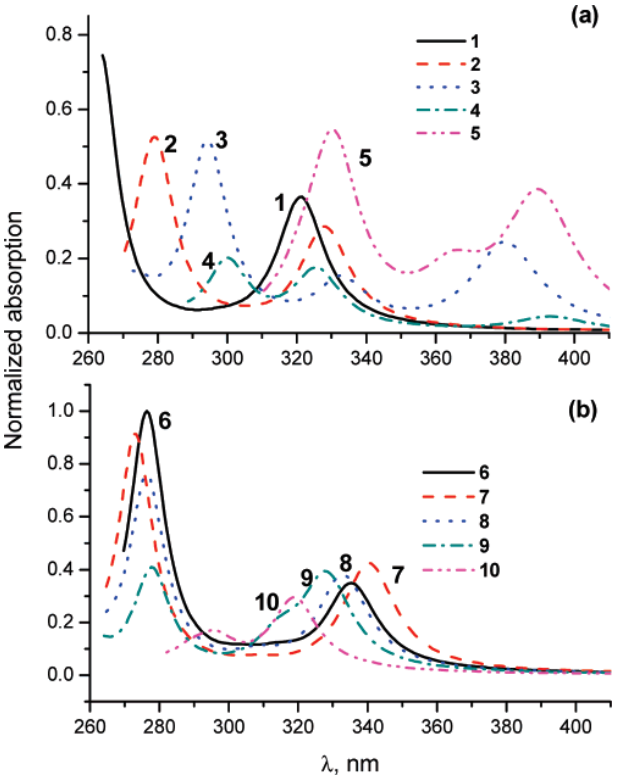

Figure 9. Calculated OPA spectra of compounds **1**−**5** (a) and **6**−**10** (b).

TABLE 4: Comparison of Theoretical and Experimental Linear (one-photon) Excitation Energies for Compounds 1−10 ("s" marks calculations which include toluene solvent)

	experiment		theory			
compound	λ nm	Ω_{OPA} eV	Ω_{OPA} eV	excited state no.	excited-state symmetry	$\mu_{g\nu}$ D
1	310	4.00	3.86	1	B	5.34
	273	4.55	4.71	3	A	7.68
2	300	4.14	3.78	1	B	4.68
	278	4.46	4.45	3	A	5.64
2s	300	4.14	3.73	1	B	4.67
	278	4.46	4.38	3	A	6.17
3	360	3.45	3.27, 3.73	1, 2	B, A	4.33, 3.11
	272	4.56	4.22	3	A	6.31
3s	360	3.45	3.21	1	B	4.29
	272	4.56	4.16	3	A	6.24
4	335	3.70	3.16, 3.81	1, 2	B, A	1.76, 3.56
	272	4.56	4.14	3	A	3.79
5	350	3.55	3.19	1	B	5.33
	315	3.94	3.76	5	A	6.32
5s	350	3.55	3.11	1	B	5.21
	315	3.94	3.65	5	A	5.82
6	315	3.94	3.7	1	B	5.14
	278	4.46	4.49	6	A	8.91
7	320	3.88	3.73	1	B	5.42
	286	4.34	4.49	3	A	7.68
8	325	3.82	3.65	1	B	5.77
	281	4.42	4.54	3	A	8.51
9	315	3.94	3.79	3	A	5.26
	313	3.96	4.47	5	A	5.35
10	305	4.07	3.89	3	A	4.71
	303	4.1	4.2	4	A	2.87

TABLE 5: Comparison of Theoretical and Experimental Two-photon Excitation Energies and Relative Cross-sections for Compounds 1−10

	Ω_{TPA}, eV	Ω_{TPA}, eV				relative TPA cross-sections	
compound	experiment	theory	no. of excited state	excited-state symmetry	σ_{TPA}, GM	experiment	theory
1	2.29	1.97	1		17		0.54
		2.6	9	A	55	0.55 ± 0.09	(0.71)
2	2.24	2.05, 2.6	2, 11	A, A	13, 19	0.37 ± 0.06	0.42
		2.23	3	A	42		(0.74)
2s[a]	2.24	2.02	2	A	15	0.37 ± 0.06	0.63
		2.19	3	A	63		(0.78)
3	2.29	1.87	2	A	60	1 ± 0.17	1.00
		2.11	3	A	101		(1.60)
3s	2.29	1.82	2	A	65	1 ± 0.17	1.06
		2.08	3	A	106		(1.70)
4	2.29	2.07	3	A	28		0.28
		2.26, 2.6	6, 11	A, A	26, 20		(0.74)
5	2.71	1.7	2	A	106.6		1.28
		1.88	5	A	129		(2.36)
5s	2.71	1.65	2	A	99		1.00
		1.82	5	A	100		(2.00)
6	2.24	1.98	2	A	12.3	0.26 ± 0.04	0.68
		2.33	7	A	69		(0.81)
7	2.2	2.04	2	A	26	0.46 ± 0.08	0.68
		2.48	8	A	69		(0.95)
8	2.2	2.02	2	A	22	0.39 ± 0.07	1.16
		2.42	7	A	117.5		(1.40)
9	2.46	1.98	4	A	13	1.34 ± 0.23	0.72
		2.23	5	A	73		(0.86)
10	2.41	2.11	4	A	15		0.18
		2.35	10	A	18		(0.33)

[a] "s" marks calculations which include toluene solvent; cumulative theoretical cross-sections are in parentheses.

is parallel to the symmetry axis, while for A−B excitations the transition dipole is orthogonal to this axis. Therefore, two peaks on OPA spectra should have different polarization.

The result of theoretical simulations for the TPA spectra are presented in Figure 10 and compared with the experimental data in Table 5. Most of the spectra have complex structure, reflecting multiple TPA-active excited states. Noticeably, the B states disappear from the picture in perfect agreement with the experiment.[46] All TPA states have the same A symmetry as the ground state, mimicking selection rules for centrosymmetric molecules. However, unlike the centrosymmetric case, the state with the largest TPA cross-section is also active (and even dominant) in the OPA spectrum. This observation can be rationalized by recalling that typically strong TPA activities are observed in the substituted chromophores in the direction of intramolecular charge transfer which would correspond to the symmetry axis in our case.

Direct comparison of theoretical results with experiment is not possible since spectroscopic measurements of the cross-sections have been performed only for a narrow spectral range and, therefore, do not provide complete information on the TPA line shapes and peak maxima. In turn, all comparisons with experiment for amplitude of the responses are subject to an uncertainty in the choice of the line-broadening parameter $\Gamma =$ 0.1 eV which may vary for real molecular systems. Moreover, multiple TPA-allowed states often mix and borrow intensity from one another, and their relative cross-sections depend strongly on computational details (such as a percentage of exact exchange in the density functional and polarity of the environment).[40,45] Subsequently, this comparison can be used only as a guideline, and Table 5 demonstrates only a modest agreement. Finally, calculations conducted in the presence of solvent (toluene) show several characteristic trends due to the dielectric environment. We observe solvatochromic red-shift excitation energies by ∼0.1 eV in all dipolar allowed A and B states. Compared to the gas-phase calculations, the solvent also

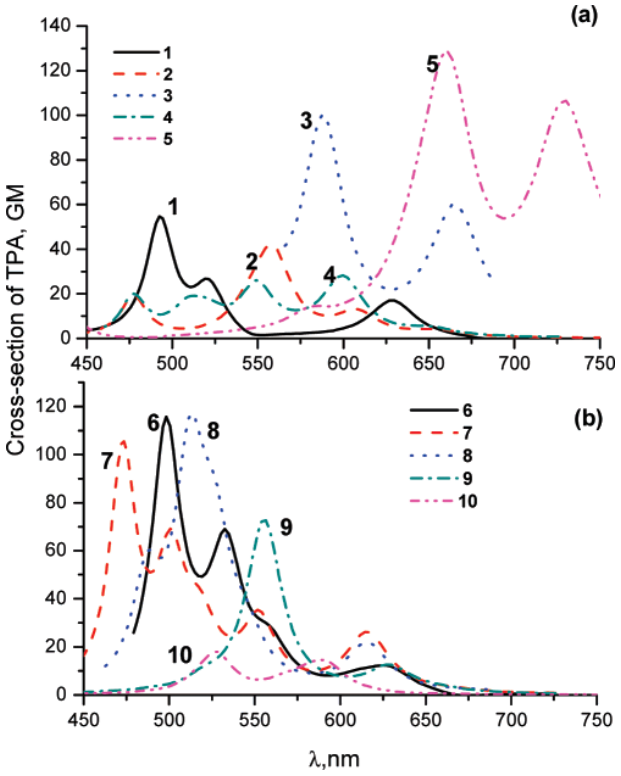

Figure 10. Calculated TPA spectra of compounds **1**−**5** (a) and **6**−**10** (b).

increases mixing among excited states, which, in turn, leads to the larger TPA cross-sections in solvent. Most importantly, our computations also suggest that the range of excitation wavelengths for TPA can be expanded to >675 nm for **3** and even to >750 nm for **5**. These predictions await an experimental confirmation.

Conclusions

We found that TPA absorption cross-sections in benzannelated enediynes increase upon the introduction of donor substituents at the core and strongly acceptor substituents at the periphery. Interestingly, related compounds, such as substituted bis(styryl)benzenes, which have acceptor−donor−acceptor (A−D−A) or donor−acceptor−donor combinations of substients show rather large TPA cross-sections.[47,48] Note, however, that geometries of these linear quadrupolar molecules differ noticeably from the angular orientation of substituents in the ortho-enediyne moiety. Less polarized enediynes do not show clear trends, but noticeable variations in the efficiency of TPA are observed. Lower fluorescence quantum yields in enediynes with a pyrazine core may indicate deactivation of the S1 state by other pathways, such as intersystem crossing[33] or a chemical reaction. For enediynes with the lowest one-photon state of B symmetry, TPA should target higher excited states.

In summary, we provided the first study of TPA behavior of enediyne chromophores in both theory and experiment. By selecting suitable substitution patterns, we can modify the TPA cross-sections. Future studies will show whether further polarization will lead to a continuous increase in TPA cross-sections. The possibility of two-photon activation paves the way for practical application of the photochemistry of enediynes in photodynamic therapy of cancer by moving the range of available wavelengths closer to the therapeutic window of tissues.

Acknowledgment. I.A. is grateful to the National Science Foundation (CHE-0316598) and to Material Research and Technology (MARTECH) Center at Florida State University for partial support of this research and to the 3M Company for an Untenured Faculty Award. The research at LANL is supported by the Center for Nonlinear Studies (CNLS) and the LDRD program of the U.S. Department of Energy. This support is gratefully acknowledged. We thank T. Zeidan and S. Peabody for preparation of several enediynes.

Supporting Information Available: Experimental procedures and spectral data for compounds **1**−**10**. Complete refs 32d and 42. This material is available free of charge via the Internet at http://pubs.acs.org.

References and Notes

(1) Jones, R. R.; Bergman, R. G. *J. Am. Chem. Soc.* **1972**, *94*, 660. Bergman, R. G. *Acc. Chem. Res.* **1973**, *6*, 25.

(2) Liu, W.; Christenson, S. D.; Standage, S.; Shen, B. *Science* **2002**, *297*, 1170. Ahlert, J.; Shepard, E.; Lomovskaya, N.; Zazopoulos, E.; Staffa, A.; Bachmann, B. O.; Huang, K.; Fonstein, L.; Czisny, A.; Whitwam, R. E.; Farnet, C. M.; Thorson, J. S. *Science* **2002**, *297*, 1173.

(3) Pogozelski, W. K.; Tullius, T. D. *Chem. Rev.* **1998**, *98*, 1089.

(4) (a) Nicolaou, K. C.; Smith, A. L. *Acc. Chem. Res.* **1992**, *25*, 497. (b) Grissom, J. W.; Gunawardena, G. U.; Klingberg, D.; Huang, D. *Tetrahedron* **1996**, *19*, 6453. (c) Wang, K. K. *Chem. Rev.* **1996**, *96*, 207.

(5) Nicolaou, K. C.; Pitsinos, E. N.; Theodorakis, E. A.; Saimato, H.; Wrasidlo, W. *Chem. Biol.* **1994**, *1,* 57−66.

(6) Incorporation of the enediyne unit into a strained 9- or 10-membered ring was shown to facilitate the reaction through ground-state destabilization. For the experimental work, see: (a) Nicolaou, K. C.; Zuccarello, G.; Ogawa, Y.; Schweiger, E. J.; Kumazawa, T. *J. Am. Chem. Soc*. **1988**, *110*, 4866. (b) Nicolaou, K. C.; Zuccarello, G.; Riemer, C.; Estevez, V. A.; Dai, W.-M. *J. Am. Chem. Soc*. **1992**, *114*, 7360. (c) IIda, K.; Hirama, M. *J. Am. Chem. Soc.* **1995**, *117*, 8875.

(7) For a theoretical analysis of the strain effects on the cyclization, see: (a) Snyder, J. P. *J. Am. Chem. Soc.* **1990**, *112*, 5367. (b) Schreiner, P. R. *J. Am. Chem. Soc*. **1998**, *120*, 4184.

(8) Kraka and Cremer found that a decrease of the 1,6-distance in **1** (as will occur if the enediyne unit is incorporated into a 9- or 10-membered ring) indeed leads to a substantial lowering of the barrier: Kraka, E.; Cremer, D. *J. Am. Chem. Soc*. **1994**, *116*, 4929.

(9) The cyclization can also be controlled by release of strain in the transition state: Magnus, P.; Carter, P. Elliott, J.; Lewis, R.; Harling, J.; Pitterna, T.; Bauta, W. E.; Fortt, S. *J. Am. Chem. Soc.* **1992**, *114*, 2544.

(10) Representative examples: Schmittel, M.; Kiau, S. *Chem. Lett.* **1995**, 953. Maier, M. E.; Greiner, B. *Liebigs Ann. Chem*. **1992**, 855. Kim, C.-S.; Russell, K. C. *J. Org. Chem.* **1998**, *63*, 8229. Jones, G. B.; Plourde, G. W. *Org. Lett.* **2000**, *2*, 1757. Hoffner, J.; Schottelius, J.; Feichtinger, D.; Chen, P. *J. Am. Chem. Soc.* **1998**, *120,* 376. Choy, N.; Kim, C.-S.; Ballestero, C.; Argitas, L., Diez, C.; Lichtenberg, F.; Shapiro, J.; Russell, K. C. *Tetrahedron Lett.* **2000**, *41*, 6955. Alabugin, I. V.; Manoharan, M.; Kovalenko, S. V. *Org. Lett.* **2002**, *4*, 1119. Alabugin, I. V.; Manoharan, M. *J. Phys. Chem. A* **2003**, *107*, 3363. Jones, G. B.; Warner, P. M. *J. Am. Chem. Soc.* **2001**, *123,* 2134. Prall, M. Wittkopp, A. Fokin, A. A.; Schreiner, P. R. *J. Comput. Chem.* **2001**, *22*, 1605. Benites, P. J.; Rawat, D. S.; Zaleski, J. M. *J. Am. Chem. Soc.* **2000**, *122*, 7208.

(11) Recent review: Nath, M.; Huffman, J. C.; Zaleski, J. M. *Chem. Commun.* **2003**, *858* and references therein.

(12) For representative recent references, see: Knoll, K.; Wrasidlo, W.; Scherberich, J. E.; Gaedicke, G.; Fischer, P. *Cancer Res.* **2000**, *60*, 6089. Schmidt, C. S.; Wrasidlo, W.; Scherberich, J. E.; Gaedicke, G.; Fischer, P. *Tumor Targeting* **2000**, *4*, 271.

(13) Kagan, J.; Wang, X.; Chen, X.; Lau, K. Y.; Batac, I. V.; Tuveson, R. W.; Hudson. J. B. *J. Photochem. Photobiol., B* **1993**, *21*, 1352.

(14) (a) Turro, N. J.; Evenzahav, A.; Nicolauo, K. C. *Tetrahedron Lett.* **1994**, *15*, 8089. (b) Evenzahav, A.; Turro, N. J. *J. Am. Chem. Soc.* **1998**, *120*, 1835.

(15) Jones, G. B.; Wright, J. M.; Plourde, G., II; Purohit, A. D.; Wyatt, J. K.; Hynd, G.; Fouad, F. *J. Am. Chem. Soc.* **2000**, *122*, 9872.

(16) Kaneko, T.; Takahashi, M.; Hirama, M. *Angew. Chem., Int. Ed.* **1999**, *38*, 1267.

(17) Funk, R. L.; Young, E. R. R.; Williams, R. M.; Flanagan, M. F.; Cecil, T. L. *J. Am. Chem. Soc.* **1996**, *118*, 3291.

(18) Choy, N.; Blanco, B.; Wen, J.; Krishan; A.; Russell, K. C. *Org. Lett.* **2000**, *2*, 3761.

(19) Note also several reports of indirect, photochemically triggered, but thermal, Bergman cycloaromatizations. (a) Wender, P. A.; Zercher, C. K.; Beckham, S.; Haubold, E.-M. *J. Org. Chem.* **1993**, *58*, 5867. Wender, P. A.; Beckham, S.; O'Leary, J. G. *Synthesis* **1994**, 1278. (b) Nicolauo, K. C.; Dai, W. M.; Wendeborn, S. V.; Smith, A. L.; Torisawa, Y.; Maligres, P.; Hwang, C. K. *Angew. Chem., Int. Ed. Engl.* **1991**, *30*, 1032. (c) Nakatani, K.; Isoe, S.; Maekawa, S.; Saito, I. *Tetrahedron Lett.* **1994**, *35*, 605. Nakatani, K.; Maekawa, S.; Tanabe, K.; Saito, I. *J. Am. Chem. Soc.* **1995**, *117,* 10635. (d) Basak, A.; Bdour, M. H.; Shain, J. S.; Mandal, S.; Rudra, K. R.; Nag, S. *Bioorg. Med. Chem. Lett*. **2000**, *10*, 1321. (e) Problems with cis−trans isomerization: König, B.; Schofield, E.; Bubenitschek, P.; Jones, P. G. *J. Org. Chem.* **1994**, *59*, 7142. (f) Photosensitized electron-transfer reactions of aromatic enediynes with formation of enediyne radical cations: Ramkumar, D.; Kalpana, M.; Varghese, B.; Sankararaman, S. Jagadeesh, M. N.; Chandrasekhar, J. *J. Org. Chem.* **1996**, *61*, 2247. (g) Poloukhtine, A.; Popik, V. V. *J. Org. Chem.* **2003**, *68,* 7833. Poloukhtine, A.; Popik, V. V. *Chem. Commun.* **2005**, 617.

(20) Benites, P. J.; Holmberg, R. C.; Rawat, D. S.; Kraft, B. J.; Klein, L. J.; Peters, D. G.; Thorp, H. H.; Zaleski, J. M. *J. Am. Chem. Soc.* **2003**, *125,* 6434.

(21) A few notable exclusions include a water-soluble dialkynylpyrene reportedby Funk et al. where ds DNA cleavage was observed after only 15 min at 20 μM enediyne concentration although using a powerful 450 W mercury lamp.[17] A recent report of Zaleski et al. showed that copper complexes of bis(pyridine) enediynes lead to a mixture of linear (form III) and nicked plasmid, with complete consumption of the supercoiled form I only after 8 h of irradiation at concentrations of enediynes in the range of 50−500 μM. At the lower concentrations, a mixture of unreacted supercoiled form I and nicked form II DNA is formed.[20a] In a recent communication (Schmittel, M.; Viola, G.; Dall'Acqua, F.; Morbach, G. *Chem. Comm*. **2003**, 646), the mixture of ds and ss DNA cleavage was observed at rather high (1 mM) enediyne concentrations after 4 h of 419 nm irradiation.

(22) Shiraki, T.; Sugiura, Y. *Biochemistry* **1990**, *29,* 9795.

(23) Alabugin, I. V.; Kovalenko, S. V. *J. Am. Chem. Soc.* **2002**, *124*, 9052.

(24) Alabugin, I. V.; Manoharan, M. *J. Am. Chem. Soc.* **2003**, *125*, 4495.

(25) Kovalenko, S. V.; Peabody, S.; Manoharan; M.; Clark, R. J.; Alabugin, I. V. *Org. Lett.* **2004**, *6*, 2457. Peabody, S.; Breiner, B.; Kovalenko, S. V.; Patil, S.; Alabugin, I. V. *Org. Biomol. Chem.* **2005***, 3*, 218. Further theoretical analysis: Alabugin, I. V.; Manoharan, M. *J. Am. Chem. Soc.* **2005**, *127,* 9534. Alabugin, I. V.; Manoharan, M. *J. Am. Chem. Soc.* **2005**, *127*, 12583.

(26) Breiner, B.; Alabugin, I. V., unpublished work.

(27) Kovalenko, S. V.; Alabugin, I. V. *Chem. Commun.* **2005**, 1444.

(28) Povirk, L. F.; Wübker, W.; Steighner, R. J. *Biochemistry* **1989**, *28*, 5808. Absalon, M. J.; Kozarich, J. W.; Stubbe, J. *Biochemistry* **1995**, *34*, 2065. **S**tubbe, J.; Kozarich, J. W.; Wu, W.; Vanderwall, D. E. *Acc. Chem. Res*. **1996**, *29*, 322. Charles, K.; Povirk, L. F. *Chem. Res. Toxicol*. **1998**, *11*, 1580.

(29) Goppert-Mayer, M. *Ann. Phys*. **1931**, *9*, 273. McClain, W. M. *Acc. Chem. Res*. **1974**, *7*, 129−135.

(30) Fisher, W. G.; Partridge, W. P.; Dees, C.; Wachter, E. *Photochem. Photobiol.* **1997**, *66*, 141−155. Bhawalkar, J. D.; He, G. S.; Prasad, P. N. *Rep. Prog. Phys.* **1996**, *59*, 1041. McIlroy, S. P.; Clo, E.; Nikolajsen, L.; Frederiksen, P. K.; Nielsen, C. B.; Mikkelsen, K. V.; Gothelf, K. V.; Ogilby, P. R. *J. Org. Chem*. **2005**, *70*, 1134. Herman, B.; Wang, X. F.; Wodnicki, P.; Perisamy, A.; Mahajan, N.; Berry, G.; Gordon, G. In *Applied Fluorescence in Chemistry, Biology and Medicine*; Retting, B. S. W., Schrader, S., Seifert, H., Eds.; Springer: New York, 1999.

(31) For other applications of two-photon activation, see: Belfield, K. D.; Ren, X.; Van Stryland, E. W.; Hagan, D. J.; Dubikovski, V.; Meisak, E. J. *J. Am. Chem. Soc*. **2000**, *122*, 1217. Denk, W.; Strickler, J. H.; Webb, W. W. *Science* **1990**, *248*, 73. Kohler, R. H.; Cao, J.; Zipfel, W. R.; Webb, W. W.; Hansen, M. R. *Science* **1997**, *276*, 2039.

(32) Compounds that exhibit large TPA cross-sections have a variety of potential applications such as 3D optical storage memory, confocal microscopy, upconversion lasing, and photodynamic therapy: (a) Dvornikov, A. S.; Rentzepis, P. M. *Science* **1989**, *245*, 843. (b) Denk, W.; Strickler, J. H.; Webb, W. W. *Science* **1990**, *248*, 73. (c) Bhawalkar, J. D.; He, G. S.; Prasad, P. N. *Rep. Prog. Phys*. **1996**, *59*, 1041. (d) Albota, M.; et al. *Science* **1998**, *281*, 1653.

(33) Zeidan, T.; Kovalenko, S. V.; Manoharan, M.; Clark, R. J.; Ghiviriga, I.; Alabugin, I. V. *J. Am. Chem. Soc.* **2005**, *127*, 4270. Zeidan, T.; Clark, R. J.; Kovalenko, S. V.; Ghiviriga, I.; Alabugin, I. V. *Chem.*−*Eur. J.* **2005**, *11,* 4953.

(34) For details on the synthesis of compounds **1**−**10**, including spectral data, see Supporting information.

(35) Artamkina, G. A.; Kovalenko, S. V.; Beletskaya, I. P.; Reutov, O. A. *Russ. J. Org. Chem.* **1990**, *26*, 225. For fluoride-induced reaction or organosilicon compounds with electron-deficient aromatic substrates, see also: (a) RajanBabu, T. V.; Fukunaga, T. *J. Org. Chem.* **1984**, *49*, 4571. (b) RajanBabu, T. V.; Reddy, G. S.; Fukunaga, T. *J. Am. Chem. Soc.* **1985**, *107*, 5473. (c) Artamkina, G. A.; Kovalenko, S. V.; Beletskaya, I. P.; Reutov, O. A. *Russ. J. Organomet. Chem.* **1987**, *329*, 139. (d) Kovalenko, S. V.; Artamkina, G. A.; Beletskaya, I. P.; Reutov, O. A. *J. Organomet. Chem.* **1988**, *1*, 125.

(36) Zhang, B. J.; Jeon, S. J. *Chem. Phys. Lett*. **2003**, *377*, 210−216.

(37) Casida, M. E. In *Recent Advances in Density-Functional Methods*; Chong, D. A., Ed.; World Scientific: Singapore, 1995; Vol. 3 of part I.

(38) Becke, A. D. *J. Chem. Phys.* **1993**, *98*, 5648.

(39) Runge, E.; Gross, E. K. U. *Phys. Rev. Lett.* **1984**, *52*, 997.

(40) (a) Masunov, A.; Tretiak, S. *J. Phys. Chem. B* **2004**, *108*, 899. (b) Kobko, N.; Masunov, A.; Tretiak, S. *Chem. Phys. Lett*. **2004**, *392*, 444. (c) Badaeva, E. A.; Timofeeva, T. V.; Masunov, A.; Tretiak, S. J. *J. Phys. Chem. A* **2005**, *109*, 7276.

(41) Katan, C.; Terenziani, F.; Mongin, O.; Werts, M. H. V.; Porres, L.; Pons, T.; Mertz, J.; Tretiak, S.; Blanchard-Desce, M. *J. Phys. Chem. A* **2005**, *109*, 3024. 201: Bartholomew, G. P.; Rumi, M.; Pond, S. J. K.; Perry, J. W.; Tretiak, S.; Bazan, G. C. *J. Am. Chem. Soc.* **2004**, *126*, 11529.

(42) Frisch, M. J.; et al. *Gaussian 98*, revision A.11; Gaussian, Inc.: Pittsburgh, PA, 1998.

(43) Tretiak, S.; Mukamel, S. *Chem. Rev.* **2002**, *102*, 3171.

(44) Tretiak, S.; Chernyak, V. *J. Chem. Phys.* **2003**, *119*, 8809.

(45) Furche, F.; Ahlrichs, R. *J. Chem. Phys.* **2002**, *117*, 7433.

(46) Wang, C.; Macak, P.; Luo, Y.; Ågren, H. *J. Chem. Phys.* **2001**, *114*, 9813.

(47) Rumi, M.; Ehrlich, J. E.; Heikal, A. A.; Perry, J. W.; Barlow, S.; Hu, Z.; McCord-Maughon, D.; Parker, T. C.; Rockel, H.; Thayumanavan, S.; Marder, S. R.; Beljonne, D.; Bredas, J.-L. *J. Am. Chem. Soc* **2000**, *122*, 9500−9510.

(48) Day, P. N.; Nguyen, K. A.; Pachter, R. *J. Phys. Chem B* **2005**, *109*, 1803.